Production of $Ni_{100-x-y}Mn_xGa_y$ magnetic shape memory alloys by mechanical alloying

2008 J. Phys.: Condens. Matter 20 445205

(http://iopscience.iop.org/0953-8984/20/44/445205)

J. Phys.: Condens. Matter **20** (2008) 445205 (8pp) doi:10.1088/0953-8984/20/44/445205

Production of $Ni_{100-x-y}Mn_xGa_y$ magnetic shape memory alloys by mechanical alloying

T D Hatchard[1,3,4], J S Thorne[1], S P Farrell[2] and R A Dunlap[1,3]

[1] Department of Physics and Atmospheric Science, Dalhousie University, Halifax, Nova Scotia, B3H 3J5, Canada
[2] Defence R&D Canada—Atlantic, PO Box 1012, 9 Grove Street, Dartmouth, Nova Scotia, B2Y 3Z7, Canada
[3] Institute for Research in Materials, Dalhousie University, Halifax, Nova Scotia, B3H 3J5, Canada

E-mail: hatchard@dal.ca

Received 13 June 2008, in final form 25 August 2008
Published 30 September 2008
Online at stacks.iop.org/JPhysCM/20/445205

Abstract

Powdered samples of a variety of compositions of the off-stoichiometric magnetic shape memory alloy Ni_2MnGa have been prepared by mechanical alloying from elemental precursors. As-milled powders are highly disordered and show very weak ferromagnetic order. Annealing produces a well-ordered $L2_1$ Heusler phase with high saturation magnetization. Annealing results in a consistent loss of Ga of about 1–4 at.% (of total sample composition). Structural and magnetic properties of a range of compositions have been measured and are reported in the present work. A magnetically oriented metal–polymer composite has been prepared by mixing the powdered sample in epoxy and curing under an externally applied magnetic field. The magnetic anisotropy energy of the composite sample has been measured and found to be about 20% of the value expected for a single crystal of similar composition. Possibilities for increasing the magnetic anisotropy of metal–polymer composites are discussed. Results are discussed in terms of the effects of structural and chemical order on the resulting magnetic properties in the context of a model based on indirect exchange interactions.

1. Introduction

Magnetic shape memory alloys have recently been studied as an alternative to the more commonly known thermal shape memory alloys for use as sensors or actuators [1–3]. These alloys are attractive as their response can be controlled by the application of magnetic fields, which can be modulated much more quickly than the temperature of a material. In particular, the Heusler alloy Ni_2MnGa is of interest due to a martensitic transition in the ferromagnetic regime [4].

In the stoichiometric Ni_2MnGa alloy, the martensitic transition occurs below room temperature, with the material being in the cubic austenite phase above 227 K [4]. However, varying the stoichiometry allows for control of materials properties such as saturation magnetization, Curie temperature and magnetic anisotropy energy in addition to the temperature of the martensite-to-austenite phase transition. For appropriate compositions, it has been shown that both the martensitic transition and the Curie transition occur above room temperature giving rise to a number of potential applications (e.g. [5, 6]). Recent studies have focused on the variation of these properties with composition in single crystal and arc melted samples [2, 3, 7–12]. These studies have shown that the properties of these materials are very sensitive to changes in composition. The overall strength of the magnetic interactions in Ni–Mn–Ga is a maximum (as evidenced by the Curie temperature) for the Heusler stoichiometry (Ni_2MnGa). It is also known that alloys with either substantially more or less Mn have lower Curie temperatures. That is, for alloys of the form $Ni_{100-x-y}Mn_xGa_y$ the Curie temperature is a maximum near $x = 25$ (the $L2_1$ Heusler stoichiometry). The majority of the magnetic moment in these alloys is carried by the Mn ions with a smaller moment associated with the Ni ions [13]. In these materials the greatest changes in the

[4] Author to whom any correspondence should be addressed.

magnetic properties will be associated with changes in Mn content, with smaller changes associated with changes in Ni (and possibly Ga) content. The reduction in Curie temperature and saturation magnetization for alloys with $x < 25$ may be a direct consequence of the dilution of the magnetic moment carrying Mn ions. For alloys with $x > 25$, Enkovaara *et al* [14] have suggested that the magnetic properties are the result of antiferromagnetic coupling of the excess Mn ions. Indirect exchange interactions between localized magnetic moments are responsible for ferromagnetic order in Heusler alloys [15, 16] and their magnetic properties [17–25] have been modeled on the basis of the resulting oscillations in the conduction band polarization.

Single crystals of Ni–Mn–Ga are expensive to prepare and, in addition, are brittle and difficult to machine and form into complex shapes. A possible economical alternative to the use of single crystals is the use of an oriented metal–polymer composite that incorporates magnetic shape memory alloy powder [26–28]. This composite could then be used as a sensor or actuator without the need for large single crystals [27, 29]. This technique requires the ability to produce large amounts of powder with known properties and subsequently to align the easy axis of magnetization within a polymer matrix. Due to the sensitivity of the properties of the material to the composition, the technique used to produce the powder must give consistent, predictable results.

The present paper reports the use of mechanical alloying (ball milling) to produce powders of $Ni_{100-x-y}Mn_xGa_y$ with $18.7 < x < 31$ and $19.2 < y < 22.7$. A summary of the properties of various compositions in the as-milled state and after annealing is given. Detailed studies are presented for one composition that is orthorhombic at room temperature. A model based on indirect exchange interactions is used to explain the details of the relationship between microstructural disorder and the resulting magnetic properties. The magnetic anisotropy of a metal–polymer composite has been measured and is considered in the context of the properties of a single crystal of similar composition.

2. Experimental methods

Powder samples were produced by mechanical alloying from elemental components. Nickel powder (99.9% purity/Alfa Aesar), manganese powder (99.9% purity/Aldrich) or chips (99.5% purity/Alfa Aesar) and gallium pieces (99.99% purity/Aldrich) were used. The manganese chips were etched in a 10% by volume nitric acid solution and then quenched with methanol to remove surface oxides. About three grams of starting materials were sealed under argon and placed in a hardened steel vial with two 7/16 inch diameter hardened steel balls. This gave a ball to sample weight ratio of approximately 4:1. Samples were milled for 8 h in a SPEX Model 8000 high-energy ball mill. Typically 50–80% of the sample was recovered after milling with the remainder coating the balls and vial. Samples were subsequently annealed under flowing argon at 800 °C for a period of 8 h.

Samples of as-milled and annealed powders were studied by x-ray diffraction (XRD) with a Siemens D-500 scanning diffractometer using Cu Kα radiation and electron microprobe (JEOL 8200) to determine structure and composition, respectively. A PAR-155 vibrating sample magnetometer (VSM) was used to measure the magnetization versus applied field for both as-milled and annealed samples in fields up to 0.8 T at room temperature. VSM samples were referenced to a Ni standard (54.4 emu g^{-1}). Differential scanning calorimetry (DSC) measurements were made over a temperature range of about −60 to 500 °C on as-milled and annealed samples using a TA Instruments Q1000 DSC. Measurements were made over several heating and cooling cycles. Thermogravimetric analysis (TGA) measurements were made using a TA Instruments TGA-51 Thermogravimetric Analyzer from room temperature to 600 °C during both heating and cooling. The Curie temperature was measured by placing a rare earth permanent magnet over the furnace, yielding an apparently lower mass for the sample in the ferromagnetic regime [30].

Samples for the determination of magnetic anisotropy energy were prepared by mixing the powder (∼20–80 mg) in a slow curing epoxy. Typical loading factors are in the 2–8% range by volume. The epoxy/powder mix was cured in a $\sim 5 \times 5 \times 5$ mm^3 aluminum mold to yield cubic samples for magnetic studies. To align the powder in the epoxy, several 1 inch diameter rare earth magnets were placed on two opposing sides of the Al mold while the sample cured. The permanent magnets provide an external field of about 0.4 T over the dimensions of the sample. The magnetic anisotropy was determined by measuring the magnetization of the sample with the applied field of the VSM both parallel and perpendicular to the field applied during the curing of the epoxy.

Table 1. Composition and structure of $Ni_{1-x-y}Mn_xGa_y$ samples prepared by mechanical alloying. Sample designations are used in figure captions and in table 2 to identify samples. Final compositions are after milling and annealing. Structures were determined at room temperature.

Sample	Starting composition	Final composition	Structure
1	$Ni_{50}Mn_{25}Ga_{25}$	$Ni_{49.9}Mn_{28.3}Ga_{21.8}$	Cubic
2	$Ni_{50}Mn_{25}Ga_{25}$	$Ni_{49.1}Mn_{28.7}Ga_{22.2}$	Cubic
3	$Ni_{50}Mn_{25}Ga_{25}$	$Ni_{49.4}Mn_{29.4}Ga_{21.2}$	Cubic
4	$Ni_{50}Mn_{25}Ga_{25}$	$Ni_{49.8}Mn_{28.3}Ga_{21.9}$	Cubic
5	$Ni_{50.5}Mn_{27}Ga_{22.5}$	$Ni_{49.8}Mn_{31}Ga_{19.2}$	Cubic
6	$Ni_{52}Mn_{24}Ga_{24}$	$Ni_{51.9}Mn_{26.9}Ga_{21.2}$	Cubic
7	$Ni_{58}Mn_{18}Ga_{24}$	$Ni_{59.9}Mn_{20.3}Ga_{19.8}$	Orthorhombic
8	$Ni_{55}Mn_{22}Ga_{23}$	$Ni_{54.9}Mn_{24.6}Ga_{20.5}$	Orthorhombic
9	$Ni_{53}Mn_{23}Ga_{24}$	$Ni_{54.5}Mn_{24.1}Ga_{21.4}$	Orthorhombic
10	$Ni_{58}Mn_{18}Ga_{24}$	$Ni_{60.9}Mn_{18.7}Ga_{20.4}$	Orthorhombic
11	$Ni_{53}Mn_{23}Ga_{24}$	$Ni_{52.4}Mn_{24.9}Ga_{22.7}$	Cubic
12	$Ni_{55}Mn_{22}Ga_{23}$	$Ni_{51.6}Mn_{27.7}Ga_{20.7}$	Orthorhombic
13	$Ni_{55}Mn_{22}Ga_{23}$	$Ni_{53.5}Mn_{24.6}Ga_{21.9}$	Orthorhombic

3. Results

3.1. Structure and properties of as-milled and annealed samples

Samples of various compositions as summarized in table 1 were made and their structure and composition measured as described above. Samples are subsequently referred to by

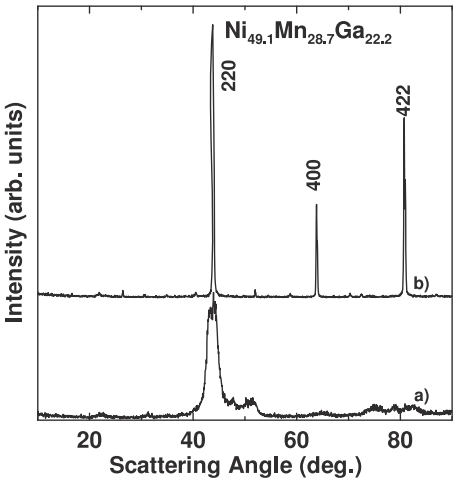

Figure 1. X-ray diffraction pattern for $Ni_{49.1}Mn_{28.7}Ga_{22.2}$ (sample 2) (a) as-milled and (b) after annealing as described in the text. The Miller indices for the diffraction peaks of the cubic $L2_1$ structure are shown in (b).

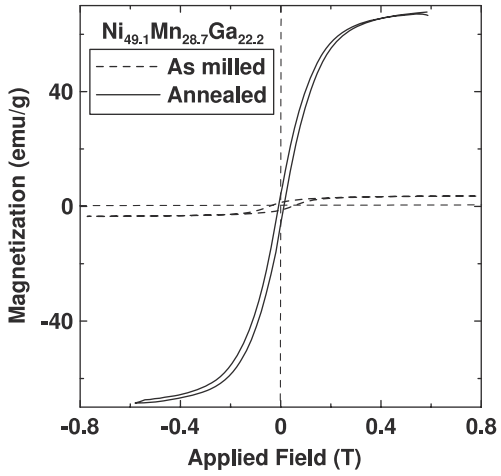

Figure 2. Magnetization versus applied field for $Ni_{49.1}Mn_{28.7}Ga_{22.2}$ (sample 2) as-milled and annealed.

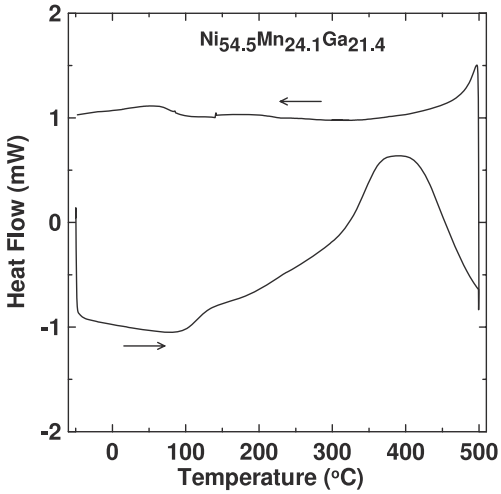

Figure 3. DSC data for $Ni_{54.5}Mn_{24.1}Ga_{21.5}$ (sample 9) as-milled. The heating and cooling directions are illustrated.

their final measured composition. These samples have been studied both as-milled and after annealing and the results are discussed in this section. The XRD pattern for a typical as-milled sample of composition $Ni_{49.1}Mn_{28.7}Ga_{22.2}$ (sample 2) is shown in figure 1(a). The pattern has broad peaks near the location of the peaks for the cubic $L2_1$ phase of Ni_2MnGa. This is typical of all as-milled powders, indicating very disordered structures with small crystallite sizes.

VSM measurements of as-milled powder samples show very low saturation magnetizations of only a few emu g^{-1}, where values of 50–70 emu g^{-1} are expected for well-ordered samples in this composition range. A typical magnetization curve for an as-milled sample, e.g. $Ni_{49.1}Mn_{28.7}Ga_{22.2}$ (sample 2), is shown in figure 2.

Figure 3 shows temperature versus heat flow for as-milled $Ni_{54.5}Mn_{24.1}Ga_{21.5}$ (sample 9) as measured by DSC. As can be seen from the figure, the onset of the ordering process is at a temperature of about 100 °C and the maximum heat flow occurs at around 400 °C. The major component of the heat flow is seen to be irreversible and does not show corresponding features on cooling.

TGA measurements of the as-milled samples did not indicate the presence of a distinct Curie temperature. This is not surprising given the very low saturation magnetization of the samples. The heat associated with crystallographic ordering obscures any evidence of the Curie temperature in the DSC scans.

Annealing of the as-milled samples greatly increases the degree of ordering. The XRD pattern for $Ni_{49.1}Mn_{28.7}Ga_{22.2}$ (sample 2) annealed at 800 °C is shown in figure 1(b). As can be seen, all peaks expected for the cubic $L2_1$ phase are now present and are very sharp, indicating large crystallite size. A very minor (unidentified) impurity phase is indicated by small peaks at (e.g.) $2\theta = 28°$ and 52°. This is typical of most samples. The results shown are for a sample that exhibits the cubic structure at room temperature after annealing but analogous results are seen for the orthorhombic samples.

Figure 2 shows the magnetization versus applied field for the annealed sample (sample 2). The magnetization of the annealed powder is very much higher than that of the as-milled sample, again indicating a much higher degree of structural ordering and this is typical of all annealed samples.

Figure 4 shows the DSC data for an annealed sample of composition $Ni_{54.5}Mn_{24.1}Ga_{21.4}$ (sample 9). This sample has a well-defined martensite-to-austenite phase transition during heating with the reverse process occurring at a slightly lower temperature during cooling. These features in the DSC scan are reversible as indicated by the inclusion of several heating/cooling cycles in the figure and are consistent with literature results for similar materials [8]. Figure 5 shows XRD patterns at three temperatures for $Ni_{54.5}Mn_{24.1}Ga_{21.4}$ (sample 9). The sample was annealed and then cooled to room temperature. It was then cooled to −50 °C and XRD patterns were collected at various times as the sample was warmed to 100 °C. At a temperature of −50 °C, the sample is in the orthorhombic phase [31]. At room temperature (about 28 °C

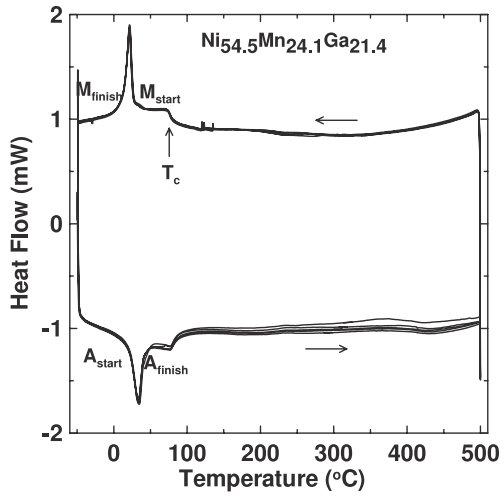

Figure 4. DSC data for $Ni_{54.5}Mn_{24.1}Ga_{21.4}$ (sample 9) after annealing. The heating and cooling directions are illustrated. The Curie temperature, T_c, and start and finish temperatures for the austenite (A_{start} and A_{finish}) and martensite (M_{start} and M_{finish}) transitions are shown.

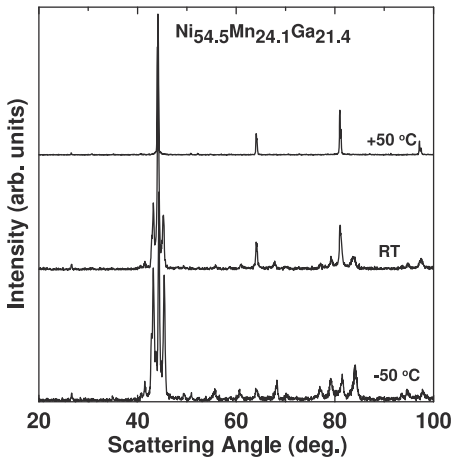

Figure 5. X-ray diffraction patterns at various temperatures for $Ni_{54.5}Mn_{24.1}Ga_{21.4}$ (sample 9) after annealing. The temperature for each pattern is indicated in the figure.

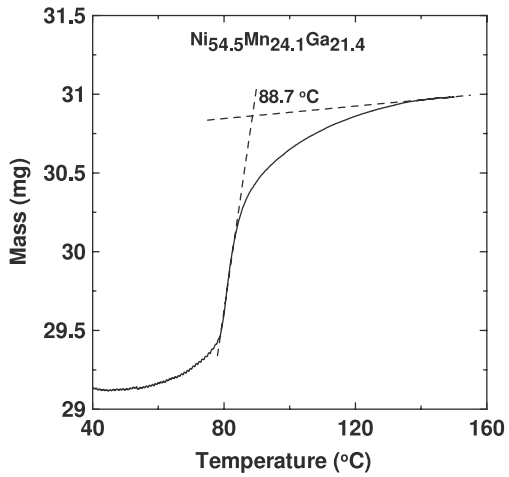

Figure 6. TGA data for $Ni_{54.5}Mn_{24.1}Ga_{21.4}$ (sample 9) after annealing. The Curie temperature is indicated as described in the text.

Table 2. Saturation magnetization, M_s, Curie temperature, T_c, and start and finish temperatures for the austenite (A_{start} and A_{finish}) and martensite (M_{start} and M_{finish}) transitions for the samples from table 1. ($*$ = not observed.)

Sample	M_s (emu g^{-1})	T_c (°C)	Transition temperatures (°C) A_{start}	A_{finish}	M_{start}	M_{finish}
1	71.7	117.2	*	*	*	*
2	73.8	110.5	−31	−8	−16	−36
3	75.1	117.9	−28	−10	−19	−39
4	73.7	107.5	−27	−7	−13	−33
5	66.0	119.9	−42	−13	−40	−60
6	60.4	92.0	−27	4	−18	−41
7	41.8	85.1	110	147	140	112
8	49.1	103.6	85	110	96	55
9	46.9	88.7	17	51	30	4
10	39.1	90.6	110	155	120	83
11	65.8	94.0	−2	31	21	−17
12	59.9	98.6	59	84	75	53
13	52.8	122.4	99	127	114	87

for this measurement), the transition is already under way, in agreement with the findings from the DSC. At 50 °C the sample is in the cubic phase. Figure 6 shows the TGA data for the $Ni_{54.5}Mn_{24.1}Ga_{21.4}$ sample from figures 4 and 5. The Curie temperature determined as in reference [30] is indicated in the figure.

The results of measurements on samples of various compositions are summarized in table 1. Both the starting compositions and the compositions measured after annealing are shown. There is generally a loss of Ga of about 1–4 at.% (of the total sample) during milling and annealing. The Mn content increases for each sample, indicating that little or no loss of Mn occurs during sample processing. The Ni content generally shows a very small decrease or an increase somewhat smaller than that for Mn, indicating that Ni loss is much smaller than Ga loss during processing. As a result a desired composition can be achieved quite closely by adjusting the initial amounts of each material in the ball mill vial.

In the present work it has been found that ball-milled samples have the cubic structure over a wider composition range than single crystal samples (see [32] and references therein). A higher Ni content is needed to produce an orthorhombic structure in ball-milled samples than in single crystals pulled from the melt. Generally, a Ni content of at least 53 at.% is needed to achieve an orthorhombic sample, with only sample 12 being an exception to this rule. The Mn and Ga contents seem to be less important in determining the crystal structure than the amount of Ni.

Table 2 summarizes the saturation magnetization, Curie temperature and structural transition temperatures for the samples from table 1. In general, saturation magnetization and Curie temperature are both lowest for those alloys with the lowest Mn content. Sample 5 suggests that excess Mn may not continue to increase the magnetization.

The cubic samples generally have martensite-to-austenite transitions beginning at around −30 °C, making them unsuitable for use in preparing magnetic shape memory alloy

metal–polymer composites for room temperature use. The orthorhombic samples have transition temperatures from as low as 17 °C to well over 100 °C. The transition temperature generally increases with Ni content, meaning that there is a trade off between a high magnetization and Curie temperature and a high structural transition temperature.

3.2. The origin and behavior of magnetic ordering

Two fundamentally important characteristics of the magnetic behavior of these alloys have been observed in the present work; (1) the very low magnetization of the as-milled samples and (2) the composition dependence of the saturation magnetization of the annealed samples. Both features share a common origin and may be described as follows in the context of the indirect exchange coupling responsible for ferromagnetic order in Heusler alloys.

The indirect exchange interaction is the result of the polarization of the conduction band and is well described by the so-called RKKY (Ruderman–Kittel–Kasuya–Yosida) oscillations [16]. The physical properties of the system that are most relevant in this approach are the spatial distribution of the localized magnetic moments, the magnitude of these moments and the overall conduction electron density. The oscillatory nature of the interaction is significant as both the magnitude and the sign of the exchange coupling may be described quantitatively in the following way.

The radial dependence of the conduction electron polarization, $p(r)$, around a localized unit magnetic moment in a free electron gas is given by [17–20, 23–25]

$$p(r) = -\frac{5}{4\pi^2 r^3}\left[\sin\delta_{\mathrm{d}}^{\uparrow}\cos\left(2k_{\mathrm{F}}r + \delta_{\mathrm{d}}^{\uparrow} + \frac{\eta}{r}\right) - \sin\delta_{\mathrm{d}}^{\downarrow}\cos\left(2k_{\mathrm{F}}r + \delta_{\mathrm{d}}^{\downarrow} + \frac{\eta}{r}\right)\right]. \quad (1)$$

Here k_{F} is the Fermi wavevector given by

$$k_{\mathrm{F}} = \frac{1}{a}\left[48\pi^2 n_0\right]^{1/3} \quad (2)$$

where a is the lattice parameter and n_0 is the average conduction electron contribution per atom in the material. In equation (1) $\delta_{\mathrm{d}}^{\sigma}$ is the d-wave phase shift for electrons of spin σ and is related to the number of spin σd-electrons by Friedel's theorem [33, 34] as

$$\delta_{\mathrm{d}}^{\sigma} = \frac{\pi}{5}Z_{\mathrm{d}}^{\sigma}. \quad (3)$$

In the above η is a preasymptotic phase factor as given by Jena and Geldart [23–25];

$$\eta = \frac{\pi a}{4}. \quad (4)$$

Following the development of Geldart and Ganguly [34] and Malmstrom *et al* [35, 36], the interaction energy between two spins, S_i and S_j, follows from the conduction electron polarization as given by equation (1) and may be written as

$$E_{ij}(r) = \frac{25\varepsilon_{\mathrm{F}}}{2\pi^2 S_i S_j}\sin\delta_{\mathrm{d}i}^{\downarrow}\sin\delta_{\mathrm{d}j}^{\downarrow}\frac{\cos\left(2k_{\mathrm{F}}r + \delta_{\mathrm{d}i}^{\downarrow} + \delta_{\mathrm{d}j}^{\downarrow} + \frac{\eta}{r}\right)}{(k_{\mathrm{F}}r)^3} \quad (5)$$

where ε_{F} is the free electron Fermi energy; $\varepsilon_f = \hbar^2k^2/(2m)$.

Calculation of the radially dependent interaction energy requires knowledge of the lattice parameter, the conduction electron density and the distribution of magnetic moments in the system. The average number of conduction electrons per atom, n_0, follows from a consideration of the electronic structure of the component ions in the alloy. The number of electrons contributed to the conduction band from each ion has been considered extensively for the Heusler alloys [17–20] and it is important to note that this is not the same as the number of electrons that is commonly used to estimate the structural stability of these alloys [5, 8]. The average conduction electron contribution per atom in an alloy of the composition $Ni_{100-x-y}Mn_xGa_y$ in terms of the electron contributions from the different elemental components is

$$n_0 = \frac{1}{100}\left[(100 - x - y)n(\mathrm{Ni}) + xn(\mathrm{Mn}) + yn(\mathrm{Ga})\right]. \quad (6)$$

The determination of the conduction electron contributions from each of the elements may be considered in terms of the known behavior of stoichiometric Heusler alloys within the context of the rigid band approximation and is discussed in detail in the appendix.

The calculation of the conduction electron contribution from Mn follows from a measurement of the Mn magnetic moment. Neutron diffraction studies have shown that Ni in stoichiometric Ni_2MnGa carries a magnetic moment of 0.24 μ_{B} [13]. Calculations presented in the literature [14] show that such a Ni moment is necessary in order to provide an overall consistent picture of the observed magnetic properties of these alloys. Therefore, the distribution of magnetic moments on the lattice sites results from the distribution of Mn and Ni ions on the lattice. As an example of the application of this model to the alloys in the present work we consider the composition of sample 4 ($Ni_{49.8}Mn_{28.3}Ga_{21.9}$). As there is an excess of Mn, it is assumed that the Y sites in the $L2_1$ structure with a composition X_2YZ are fully occupied with Mn. As the Ni composition is only slightly less that the stoichiometric Heusler composition it is also assumed that all Ni occupies X sites and most of the excess Mn resides on the Z sites (normally occupied by Ga, which is deficient in the present alloy). Enkovaara *et al* [14] have speculated that the excess Mn on Ga sites couples antiferromagnetically with the Mn residing on the Mn sites and that the small Ni moments couple ferromagnetically with the Y site Mn. Webster [4] has shown that the low temperature, high field magnetization of Ni_2MnGa as measured in the non-cubic regime provides a reliable measure of the saturation moments in this system. On the basis of neutron diffraction studies of stoichiometric Ni_2MnGa [13] and low temperature magnetization studies of alloys with similar compositions [37] it is assumed that the Ni moments are 0.24 μ_{B} and the Mn moments are 4.03 μ_{B}.

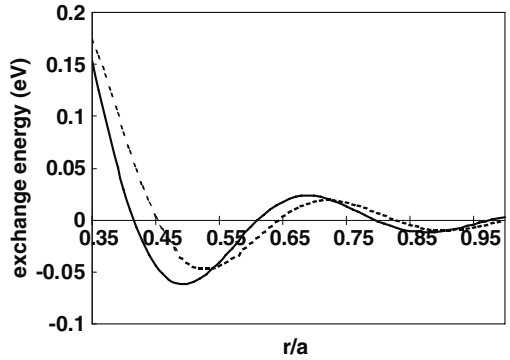

Figure 7. Exchange coupling energy in the cubic Heusler phase of $Ni_{49.8}Mn_{28.3}Ga_{21.9}$ (sample 4) as a function of distance, r, relative to the lattice parameter, a, for Mn–Mn coupling (solid line) and Mn–Ni coupling (broken line).

The radially dependent Mn–Mn and Mn–Ni exchange energy may be obtained on the basis of equation (5) and for the alloy $Ni_{49.8}Mn_{28.3}Ga_{21.9}$ the results are illustrated in figure 7. For the other alloys studied here the results are, more or less, identical to those shown in the figure. The interaction between nearest neighbor magnetic moments within a distance of one lattice parameter ($a = 0.582$ nm for the present alloy) is determined on the basis of the atomic distances given in table 3. An inspection of figure 7 along with table 3 shows the following signs for the exchange coupling of Mn with Mn or Ni on different lattice sites:

- Mn(Y)–Mn(Y)—positive.
- Mn(Y)–Mn(Z)—negative.
- Mn(Y)–Ni(X)—positive.

These results show that Mn on the Heusler Y sites will couple ferromagnetically (positive exchange coupling) with other Mn on Y sites, antiferromagnetically (negative exchange) with Mn on Z sites and ferromagnetically with Ni on X sites.

The results of the above analysis may be applied to a description of both the composition dependence of the magnetization as well as the effects of mechanical alloying on the magnetic properties. In general the hypothesis of Enkovaara *et al* [14] that Mn ions that reside on Ga sites will couple antiferromagnetically with Mn on Mn sites has been shown to be consistent with a detailed analysis of indirect exchange coupling in these alloys. Thus it is readily seen that if the Mn content of the alloy significantly exceeds that of the Heusler stoichiometry, Ni_2MnGa, then at least some excess Mn will most likely reside on Ga sites and will give rise to a reduction in the net magnetization that results from the antiferromagnetic alignment of some Mn moments.

The effects of disorder follow from this analysis. Any redistribution of Mn ions on sites other than those occupied in the 'ideal' Heusler phase as a result of chemical disorder will give rise to a reduction in the overall magnetization. While the effects of structural disorder are not readily modeled in a quantitative manner, it is clear from figure 7 that the Mn–Mn distance ($r/a = 0.707$) in the ideal Heusler structure is near the maximum in the exchange energy for ferromagnetic Mn–Mn coupling (solid line in the figure). Thus any substantial changes in Mn–Mn distances resulting from structural disorder in the Heusler phase will likely give rise to a decrease in the net magnetization. The mechanically alloyed samples are an extreme case of this behavior as they show almost no net magnetization and give rise to the conclusion that the mechanical stresses introduced during milling are, in the Ni–Mn–Ga system, sufficient to produce chemical and/or structural disorder that are manifested by significant changes in magnetic properties. The sensitivity of the Ni–Mn–Ga system to these effects is illustrated by the present work as well as previous work on the effects of plastic deformation by Imashev *et al* [38]. This behavior is in contrast to the relative insensitivity of the magnetic properties of Fe_3Ga to ball milling [39].

Table 3. Nearest neighbor shells for distances up to one lattice parameter relative to the location of a Y site ion in the $L2_1$ Heusler structure. Neighbor shells relative to X and Z site ions are given by appropriate cyclic permutations of the data in the table.

Shell	Distance (r/a)	Neighbors
1	0.433	8X
2	0.500	6Z
3	0.707	12Y
4	0.829	24X
5	0.866	8Z
6	1.000	6Y

3.3. Magnetic anisotropy

For a magnetic shape memory alloy to be useful for sensor or actuator applications it must have high magnetic anisotropy energy. Thus the material must be both non-cubic and ferromagnetic at room temperature. Sample 9 ($Ni_{54.5}Mn_{24.1}Ga_{21.4}$) was selected for the preparation of metal–polymer composites and for the measurement of magnetic anisotropy. This is the sample for which results are presented in figures 4–6.

Figure 8 shows the magnetization as a function of applied field data for the cube of metal–polymer composite containing sample 9. Data for the annealed powder are also shown for comparison. In the figure, measurements referred to as 'parallel' were made with the applied field in the VSM parallel to the direction of the field that was applied during the curing of the epoxy. Measurements referred to as 'perpendicular' were made with the applied field in the VSM perpendicular to the direction of the field that was applied during the curing of the epoxy and parallel to one of the cube edges. The application of a magnetic field during the curing of the epoxy has aligned the easy axis of magnetization of some of the crystallites in the powder resulting in the observed anisotropy. This illustrates that the powder particles, although presumably not single crystallites, do have some preferred crystallographic orientation.

The magnetic anisotropy energy is given as the area between the parallel and perpendicular magnetization curves for the positive field direction. Increasing and decreasing field curves have been averaged to eliminate the effects of hysteresis and the area has been calculated using a Simpson's

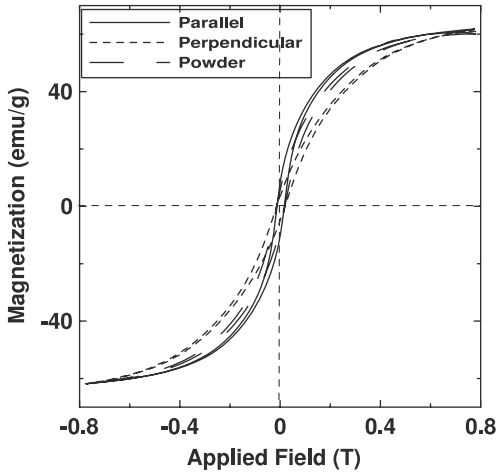

Figure 8. Magnetization versus applied field for oriented composite of $Ni_{54.5}Mn_{24.1}Ga_{21.4}$ (sample 9) and the annealed powder. The labels parallel, perpendicular and powder are described in the text. Data are scaled to account for the loading factor of the composites.

Rule integration routine. From figure 8 a magnetic anisotropy of 3.53×10^4 J m^{-3} was obtained for sample 9. This is about 20% of the value reported for single crystals of similar composition [32].

The anisotropy studies indicate that a certain degree of crystallographic texture exists within the powder grains. The measured anisotropy energy of the aligned composite is about 20% of that for a single crystal of similar composition. It may be possible to increase the anisotropy energy of the metal–polymer composite in three ways. First, the composition of the sample could be optimized to find the highest anisotropy between the easy and hard axes.

Second, it is expected that the individual powder particles are made up of clumps of crystallites. The easy axes of all crystallites within a powder particle are not necessarily all aligned with each other, so that even if the average of the easy axes of all particles are aligned with each other, the overall anisotropy will not be a maximum. In-field annealing or annealing the powder under stress could increase the crystallographic texture of the particles and, therefore, the anisotropy of the sample could be maximized by aligning the particles in the manner employed in this study. A similar approach has been shown to be productive [27] in producing magnetically oriented composites.

A third way to maximize the anisotropy energy would be to produce a tetragonal sample. Many of the single crystals reported in the literature are tetragonal as opposed to orthorhombic. In tetragonal samples, there is no distinction between the two non-easy axes while in orthorhombic samples there are two inequivalent non-easy axes; a hard axis and an intermediate axis. The easy axes of the powder grains can be aligned along the direction of the applied field during the curing of the epoxy containing the powder. However, there will be a random distribution of non-easy axes perpendicular to the field direction. This means that the curve labeled perpendicular in figure 8 is really a mix of hard and intermediate axes. A tetragonal sample may show a higher anisotropy between the easy axis and a distribution of non-easy axes. The composition range for tetragonal phases is fairly narrow and thus far single-phase tetragonal samples have not been produced by ball milling.

4. Conclusions

In summary, the present studies have shown that mechanical alloying from elemental components is a viable means for the preparation of Ni–Mn–Ga magnetic shape memory powders with structure and magnetic properties that are characteristic of the target composition. The effects of annealing have been presented and magnetic properties of as-milled and annealed samples may be explained in the context of indirect exchange interactions between Mn magnetic moments. The powder particles are shown to exhibit a reasonable degree of crystallographic texture and the present results indicate that this approach shows promise for the production of useful metal–polymer composites.

Acknowledgments

This work was funded by Defence R&D Canada—Atlantic, the Natural Sciences and Engineering Research Council of Canada and the Killam Trusts. The authors are grateful to G Fisher, I Keough, M Stancescu, A E George, E Dunlap and D J W Geldart for their contributions to this work.

Appendix. Conduction electron contributions

The conduction band contribution for each of the elements in the present alloys maybe described as follows:

Nickel: Mayo and Dunlap [19] have suggested a conduction band contribution of 0.1 electrons per Ni atom in Heusler alloys. This value has provided excellent agreement with hyperfine field systematics in Ni_2MnGa.

Manganese: The localized magnetic moment, μ(Mn), associated with a Mn ion is given (in μ_B) as the difference in the number of spin up d-electrons, $Z_d^{\uparrow}$, and the number of spin down d-electrons, $Z_d^{\downarrow}$, as

$$\mu = Z_d^{\uparrow} - Z_d^{\downarrow} \tag{7}$$

and corresponds to a net Mn spin of $S = \mu/2$. For Mn (electron configuration [Ar]$3d^5 4s^2$) the Friedel sum rule [35] gives the conduction band contribution per Mn ion as

$$n(\mathrm{Mn}) = 7 - Z_d^{\uparrow} - Z_d^{\downarrow} \tag{8}$$

Caroli and Blandin [40] have considered the simple assumption that in cases where the magnetic moment is large then one sub-band is filled [e.g. $Z_d^{\uparrow} = 5$]. However, for Ni_2MnGa and related Heusler alloys, Jha *et al* [20] have suggested that $Z_d^{\uparrow} = 4.5$ is more appropriate and have shown that this provides good agreement with experiment for a variety of hyperfine magnetic fields in a variety of different Heusler hosts. Combining equations (7) and (8) gives

$$n(\mathrm{Mn}) = \mu - 2 \tag{9}$$

Gallium: For Ga the standard sp electron configuration has been assumed: [Ar]$3d^{10}4s^2 4p^1$ giving n(Ga) = 3.

References

[1] Farrell S P, Dunlap R A, Hyatt C V and Cheng L M 2004 *Proc. SPIE* **5387** 186
[2] Jin X, Marioni M, Bono D, Allen S M and O'Handley R C 2002 *J. Appl. Phys.* **81** 8222
[3] Koho K, Söderberg O, Lanska N, Ge Y, Liu X, Straka L, Vimpari J, Heczko O and Lindroos V K 2004 *Mater. Sci. Eng.* A **378** 384
[4] Webster P J 1968 The magnetic and chemical structures of heusler alloys *PhD Thesis* University of Sheffield
[5] Wu S K and Yang S T 2003 *Mater. Lett.* **57** 4291
[6] Zhou X, Li W, Kunkel H P and Williams G 2005 *J. Magn. Magn. Mater.* **293** 854
[7] Cherechukin A A, Dikshtein I E, Ermakov D I, Glebov A V, Koledov V V, Kosolapov D A, Shavrov V G, Tulaikova A A, Krasnoperov E P and Takagi T 2001 *Phys. Lett.* A **291** 175
[8] Lanska N, Söderberg O, Sozinov A, Ge Y, Ullakko K and Lindroos V K 2004 *J. Appl. Phys.* **95** 8074
[9] Murray S J, Marioni M A, Kukla A M, Robinson J, O'Handley R C and Allen S M 2000 *J. Appl. Phys.* **87** 5774
[10] Pirge G, Hyatt C V and Altintaş S 2004 *J. Mater. Proc. Technol.* **155/156** 1266
[11] Cheng L M, Landry G, Farrell S P, Ham-Su R and Hyatt C V 2004 *Proc. MRS* **855E** W2.3.1
[12] Cheng L M, Landry G, Farrell S P, Ham-Su R and Hyatt C V 2004 *Proc. SPIE* **5387** 137
[13] Brown P J, Bargawi A Y, Crangle J, Neumann K U and Ziebeck K R A 1999 *J. Phys.: Condens. Matter* **11** 4715
[14] Enkovaara J, Heczko O, Ayuela A, Nordstrom L and Nieminen R M 2003 *Phys. Rev.* B **67** 212405
[15] White R M 1970 *Quantum Theory of Magnetism* (New York: McGraw-Hill) pp 197–200
[16] Kittel C 1996 *Introduction to Solid State Physics* 7th edn (New York: Wiley) p 628
[17] Dunlap R A and Stroink G 1982 *Can. J. Phys.* **60** 909
[18] Dunlap R A and Jones D F 1982 *Phys. Rev.* B **26** 6013
[19] Mayo W R and Dunlap R A 1982 *J. Appl. Phys.* **52** 8082
[20] Jha S, Seyoum H M, Julian G M, deMarco M, Shenoy G K and Dunlap R A 1985 *Phys. Rev.* B **32** 6104
[21] Blandin A and Campbell I A 1973 *Phys. Rev. Lett.* **31** 51
[22] Campbell I A and Blandin A 1975 *J. Magn. Magn. Mater.* **1** 1
[23] Jena P and Geldart D J W 1973 *Phys. Rev.* B **7** 439
[24] Jena P and Geldart D J W 1974 *Solid State Commun.* **15** 139
[25] Jena P and Geldart D J W 1978 *J. Magn. Magn. Mater.* **8** 99
[26] Feuchtwanger J, Griffin K, Huang J K, Bono D, O'Handley R C and Allen S M 2004 *J. Magn. Magn. Mater.* **272–276** 2038
[27] Scheerbaum N, Hinz D, Gutfleisch O, Müller K H and Schultz L 2007 *Acta Mater.* **55** 2707
[28] Hinz D, Scheerbaum N, Gutfleisch O, Müller K H and Schultz L 2007 *J. Magn. Magn. Mater.* **310** 2785
[29] Feuchtwanger J, Michael S, Juang J, Bono D, O'Handley R C, Allen S M, Jenkins C, Goldie J and Berkowitz A 2003 *J. Appl. Phys.* **93** 8528
[30] TA Instruments, Inc. *Technical note TS-37* http://www.tainst.com
[31] Bennett J C, Hyatt C V, Gharghouri M A, Farrell S, Robertson M, Chen J and Pirge G 2004 *Mater. Sci. Eng.* A **378** 409
[32] Marioni M A, O'Handley R C, Allen S M, Hall S R, Paul D I, Richard M L, Feuchtwanger J, Peterson B W, Chambers J M and Techapiesancharoenkij R 2005 *J. Magn. Magn. Mater.* **290/291** 35
[33] Friedel J 1952 *Phil. Mag.* **43** 153
[34] Geldart D J W and Ganguly P K 1970 *Phys. Rev.* B **1** 3101
[35] Malmstrom G, Geldart D J W and Blomberg C 1976 *J. Phys. F: Met. Phys.* **6** 233
[36] Malmstrom G, Geldart D J W and Blomberg C 1976 *J. Phys. F: Met. Phys.* **6** 1953
[37] Dunlap R A and Farrell S P 2008 at press
[38] Imashev R N, Mulyukov K Y, Koledov V V and Shavrov V G 2005 *J. Phys.: Condens. Matter* **17** 2129
[39] Gaudet J M, Hatchard T D, Farrell S P and Dunlap R A 2008 *J. Magn. Magn. Mater.* **320** 821
[40] Caroli B and Blandin A 1966 *J. Phys. Chem. Solids* **27** 503